Grid-independent large-eddy simulation using explicit filtering

By S. T. Bose, P. Moin AND D. You

1. Motivation and objectives

Large-eddy simulation (LES) directly solves for large-scale motions in turbulent flow, while modeling the influence of small-scale eddies. Recent studies have shown that LES provides a tractable method for the simulation of turbulent flows at high Reynolds numbers in complex geometries (Mahesh *et al.* 2006; You *et al.* 2007). The governing LES equations of LES are derived by the application of a low-pass filter, G, to the Navier-Stokes equations:

$$\bar{u}_i(x_i,t) = \int_\Omega G(x-x')u_i(x_i')dx_i' \,, \tag{1.1}$$

$$\frac{\partial \bar{u}_i}{\partial t} + \frac{\partial \bar{u}_i\bar{u}_j}{\partial x_j} = -\frac{\partial \bar{p}}{\partial x_i} + \frac{1}{Re}\frac{\partial^2 \bar{u}_i}{\partial x_j \partial x_j} - \frac{\partial \tau_{ij}}{\partial x_j} \,, \tag{1.2}$$

$$\frac{\partial \bar{u}_i}{\partial x_i} = 0 \,, \tag{1.3}$$

where $\tau_{ij} = \overline{u_i u_j} - \bar{u}_i\bar{u}_j$. Although the filtering operation is unambiguously defined in deriving Eq.1.2, in most numerical simulations the filter is not defined. It is assumed that the attenuation of high wavenumbers present in most finite difference/ finite volume schemes acts as a low pass filter (Rogallo & Moin 1984):

$$\frac{d}{dx}\left(\frac{1}{2\Delta x}\int_{x_{i-1}}^{x_{i+1}} u dx\right) = \frac{u_{i+1}-u_{i-1}}{2\Delta x} = \left.\frac{d\bar{u}}{dx}\right|_i \tag{1.4}$$

Thus, if provided a closure model for the subgrid stress tensor, $\tau_{ij} = f(\bar{u}_i, \bar{u}_j)$ and an initial condition for $\bar{u}_i$, it is possible to advance the solution for the filtered variables in time without defining the filtering operation. However, Lund (2003) has shown that the equivalence of discretized operators and filtering is inconsistent with the derivation of filtered Navier-Stokes equations. One of the difficulties associated with the arguments for "implicitly filtered" LES is that the filtering is only performed in the direction that the derivative (or interpolation) is applied. Hence, each term in the LES equation is subjected to a different 1-D filter, and the actual equation being solved cannot be rigorously derived from the Navier-Stokes equations. Due to the inherent dependence of the filtering operation on the discretized operators, it is not surprising that solutions of "implicitly filtered" LES are extremely sensitive to the numerical grid used. These issues have been highlighted by Kravchenko & Moin (2000), Meyers & Sagaut (2007), and others who counterintuitively found that agreement with direct numerical simulation or experimental data became worse when grid refinement was used. In practice, a sequence of solutions is obtained on successively finer meshes until a sufficient number of scales

in the flow field has been resolved such that the statistical quantities of interest are invariant with respect to the mesh. This is often referred to as grid convergence. However, the grid converged solution of the implicitly filtered LES is not the true solution of the LES equations. Rather, the true LES solution corresponds to the filtered velocity field calculated given a particular closure model and a well defined spatial filter. In the limit when the mesh size is sufficiently small to capture the smallest scale motion, an implicit filtered LES will converge to a direct numerical simulation because the filter width also tends to the size of the smallest eddy.

LES is also particularly sensitive to numerical errors. In most numerical simulations of physical phenomena, the detrimental impact of numerical errors can be avoided by choosing the mesh size to be much smaller than the smallest dynamically relevant length scale. This is difficult or impossible for finite difference/finite volume approaches. Kravchenko & Moin (1997) demonstrated that the performance of the subgrid stress model could be impeded due to the truncation error as the higher wavenumbers of the energy spectrum became distorted. *A priori* analyses of direct numerical simulation data of stably stratified shear flow demonstrated that both the truncation error and aliasing error associated with a numerical scheme could independently dominate the contribution of the subgrid stress tensor (Chow & Moin 2003).

Explicit filtering emerged a decade ago in order to separate the filtering and discretization operators. However, several difficulties impeded its widespread implementation. In the derivation of the Navier-Stokes equation, the filtering operation is assumed to commute with differentiation, and thus, any explicit filter used in a numerical simulation must also commute with differentiation. Vasilyev *et al.* (1998) derived filters that can commute with differentiation on nonuniform meshes to the order of accuracy of the numerical scheme. Further development of this general class of commuting filters by Marsden *et al.* (2002) and Haselbacher & Vasilyev (2003) have extended their applicability to unstructured meshes.

To date, only a handful of explicit filtered LES simulations have been performed. Initial use of explicit filtering in LES was in conjuction with solving an inverse problem for the unfiltered variables, u_i, from the filtered quantities, $\bar{u}_i$. Winckelmans *et al.* (2001) implemented a 2-D explicit filter for isotropic turbulence and a channel flow in evaluating the performance of various mixed models. Stolz & Adams (2001) implemented the filtering schemes of Vasilyev *et al.* in using an approximate deconvolution model for the convective term in the LES equations. Lund (2003) implemented two dimensional explicit filters for a channel flow and evaluated the performance of explicit filtering versus implicitly filtered LES for a variety of models. Gullbrand (2003) attempted the first grid-independent solution of the LES equations with explicit filtering. However, the explicit filter used on the finer meshes failed to commute and the statistics obtained were not conclusively grid-independent.

The objective of the present study is to obtain grid-independent solutions of the governing equations for large eddy simulation. It should be noted that the performance of explicit filtered LES with respect to direct numerical simulation is not relevant to this discussion. If the grid-independent solution of the explicit filtered LES equations fails to accurately predict the filtered DNS flow field, its failure can be solely attributed to the capability of the subgrid stress model employed. Section 2 constructs the mathematical framework for explcit filtered LES, Section 3 presents results from explicit filtered LES of a turbulent channel flow at different Reynolds numbers, and concluding remarks are presented in Section 4.

2. Mathematical framework

2.1. *Explicit filtered LES*

The convective term in the governing equations for LES can be recast in an equivalent form:

$$\frac{\partial \bar{u}_i}{\partial t} + \frac{\partial \overline{\bar{u}_i \bar{u}_j}}{\partial x_j} = -\frac{\partial \bar{p}}{\partial x_i} + \frac{1}{Re}\frac{\partial^2 \bar{u}_i}{\partial x_j \partial x_j} - \frac{\partial \tau_{ij}}{\partial x_j} \,, \tag{2.1}$$

$$\tau_{ij} = \overline{u_i u_j} - \overline{\bar{u}_i \bar{u}_j} \tag{2.2}$$

with the remaining condition that filtered velocity field, $\bar{u}_i$, is solenoidal. The primary motivation for using this form of the convective term is that a filtering operation is applied to the non-linear product $\bar{u}_i \bar{u}_j$, thereby forcing an explicit definition of the filter applied in deriving the LES equations. Moreover, the filtering operator is no longer implicitly defined by the particular grid used, and filtering and discretization operations are formally separted. A remaining constraint on the filtering operator is that it must commute with differentiation:

$$\left[\frac{\partial f}{\partial x}\right] = \frac{\overline{\partial f(x)}}{\partial x} - \frac{\partial \overline{f(x)}}{\partial x} = 0 \,. \tag{2.3}$$

Vasilyev *et al.* (1998) proposed a discrete filtering operation of the form:

$$\frac{1}{\Delta} G(x', x) = \sum_{j=-K}^{L} w_j \delta(x' - j\Delta) \,, \tag{2.4}$$

$$(G * \phi)_i = \overline{\phi}_i = \sum_{j=-K}^{L} w_j \phi_{i+j} \tag{2.5}$$

that does not satisfy Eq.2.3 exactly, but can satisfy the commutation condition to an arbitrary order of accuracy, $\left[\frac{\partial f}{\partial x}\right] = O(\tilde{\Delta}^p)$. The order of commutation, p, is typically chosen to be the same order of the truncation error of the numerical scheme used and $\tilde{\Delta}$ corresponds to the uniform grid spacing in the mapped space. The discrete filter operator in Eq.2.5 was shown to commute on non-uniform meshes by defining a transformation from the physical space to a uniformly-spaced computational space, and then performing the filtering operation in the computational space.

In the above derivation, the choice of the filter is arbitrary provided that it commutes with differentiation. However, the choice of the particular filter kernel, $G(x', x)$, is motivated by consideration of the inherent numerical error. Standard finite difference and finite volume operators have large numerical errors that are concentrated at high wavenumbers, and thus the filter kernel can be chosen in order to damp high wavenumbers that would be contaminated by the truncation error. Figure 1 shows the modified wavenumbers for a fourth order central difference operator and a hypothetical cutoff filter; the filter cutoff depicted can preserve the range of wavenumbers that are adequately resolved by the discrete difference operator, and damp the higher wavenumbers, thereby reducing the influence of numerical errors on the simulation. Ghosal (1996) used a similar modified wavenumber analysis assuming a von Karman energy spectrum in concluding that for a second-order finite-difference scheme, the filter width should be eight times

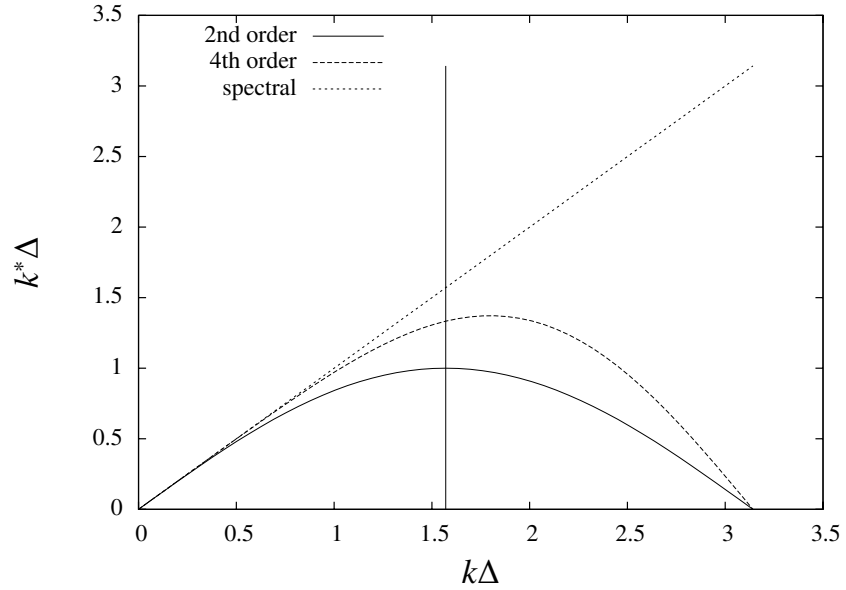

FIGURE 1. Modified wavenumbers for a second-order central difference and fourth-order central difference shown with a hypothetical cutoff filter at $k\Delta = \frac{1}{2}$.

wider than the local grid spacing, and twice as wide for an eigth-order difference scheme, in order to remove the influence of numerical error from the simulation.

Using this explicit filtering framework, it is possible to search for solutions to the LES equations that are independent of the resolution of the grid. A physical filter width is specified (for instance, a Δx_i^+ for wall-bounded flows), and an explicit filter is applied to the LES equations to only preserve the scales larger than the filter width. The mesh can then be refined in order to make the contribution from numerical errors to be small in comparison to the resolved physical scales until a solution independent of the grid used is achieved. This convergent solution is the "true" LES solution for that corresponding filter (width) and choice of subfilter closure model.

This particular form of the LES equations is not new; Biringen & Reynolds (1981) and Moin & Kim (1982) both utilized this convective form in order to exploit the fact that the Leonard stresses could be directly calculated from the filtered velocity variable. Further, this definition of explicit filtered LES is different from the approach where primitive variables are explicitly filtered at the end of each time step. The latter is inconsistent with the governing equations for LES (for a more complete discussion, see (Lund 2003). One potential drawback of using Eq.2.1 is that it is not necessarily invariant under Galilean transformation (Spezilae (1985)), although it is possible to choose a subgrid stress model such that the invariance is restored (Stolz *et al.* 2001; Gullbrand 2003).

2.2. *Numerical method*

The test case considered in this study is the turbulent, planar channel flow (Kim *et al.* 1987; Moser *et al.* 1999). This particular flow configuration is chosen because it is wall bounded, but the geometry is simple enough that a physical filter width could be fixed for different grids without undue difficulty. The fourth-order finite-difference scheme advocated by Morinishi *et al.* (1998) was implemented in a staggered mesh formulation and

the convective term is computed in its skew-symmetric form in order to discretely conserve kinetic energy. The time integration is performed using the fractional step method of Dukowicz & Dvinsky (1992) with the wall normal diffusion terms treated implicity with a Crank-Nicholson scheme, while the remaining terms were advanced with a second order Adams-Bashforth scheme.

Fourth order commuting, discrete filters derived by Vasilyev *et al.* were used to perform the explicit filtering of the convective term. The discrete 1-D filter used for the coarsest mesh was identical to the one implemented by Gullbrand:

$$\overline{\phi}_i = -\frac{1}{32}\phi_{i-3} + \frac{9}{32}\phi_{i-1} + \frac{1}{2}\phi_i + \frac{9}{32}\phi_{i+1} - \frac{1}{32}\phi_{i+3} \tag{2.6}$$

The 3-D filtering operation is then treated as a tensor product of the three 1-D filters shown in Eq.2.6. The grid distribution in the streamwise and spanwise directions are uniform with grid spacing, Δ_p, but the wall-normal grid distribution is non-uniform. Since the filtering operation is derived to be applied in a uniformly distributed computational space, ζ, the non-uniform distribution of points in physical space results in a non-uniform filter width in the wall normal direction. The distribution of grid points in the wall-normal direction is given by a hyperbolic tangent stretching function:

$$y(j) = -\frac{\tanh\left(\gamma(1-2j/N_2)\right)}{\tanh(\gamma)} \qquad j = 0, \cdots, N_2\ , \tag{2.7}$$

where N_2 and γ are the number of grid points in the wall normal direction and a mesh stretching parameter, respectively. Figure 2 depicts the Fourier transform of the filter functions used for the channel simulations. The discrete filters implemented are a smooth approximation to the spectral cutoff filter. The damping of the higher wavenumbers, $\hat{G}(\frac{\Delta k}{\pi}) > \frac{1}{2}$, has the effect of de-aliasing the convective term and damping the contributions of wavenumbers that are contaminated by the truncation error. As the mesh is refined from the coarsest mesh to the finer meshes, the filter width in Eq.2.6 fixed. The width of the filter with respect to the local grid spacing has been the subject of discussion (Lund 1997). Typically, the second moment of the filter is used as the effective filter as a measure of the width of a filter (Leonard 1973); in the case of high-order commuting filters, the second-order moment of the filter is zero. However, for filters that commute with orders of accuracy greater than two, the second order moment is zero. Instead, all the filters are computed so that the transfer functions in Fourier space are identical, thereby resolving the same scales on different grids (see Figure 2).

Asymmetric filtering is implemented in the wall-normal direction near the boundaries. The constraint that the filters commute to the same order as the truncation is enforced near the boundaries, but the shape of the transfer function is sacrificed. Because the filter stencil is no longer symmetric, it is noted that the filtering operation introduces a phase shift, although the effect of asymmetric filtering in the wall-normal direction would be minor in well-resolved LES. this has LES solution. An example of the asymmetric filter transfer function is shown in Figure 3.

A dynamic Smagorinsky subfilter stress model is used in all channel flow simulations (Germano *et al.* 1991). Because the subfilter stress term, $\tau_{ij} = \overline{u_i u_j} - \overline{u}_i \overline{u}_j$, is different from the standard subgrid term in "implicit filtered" LES, the Germano identity is modified as:

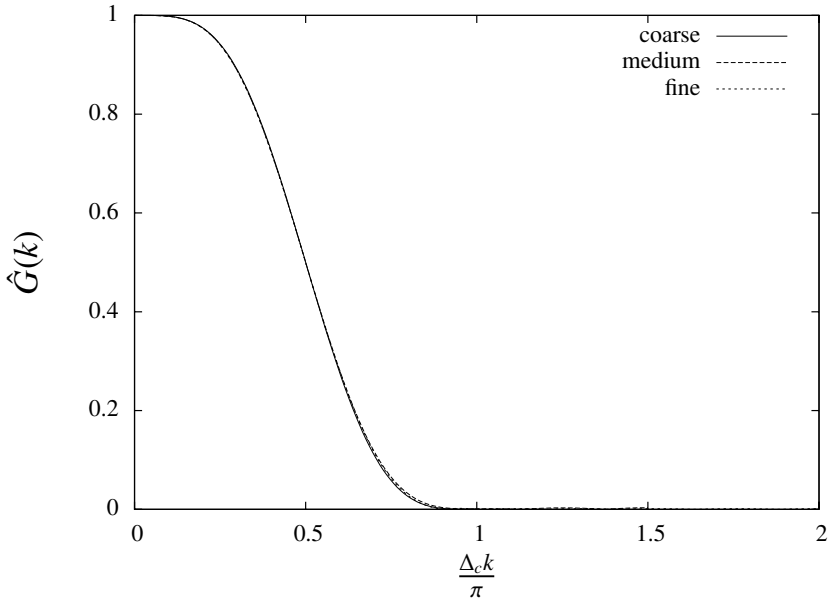

FIGURE 2. Fourier transform of filter functions $\hat{G}(k)$ with respect to a nondimensional wavenumber for a coarse grid, $\Delta_c k$. Medium grid, $\Delta_m = \frac{2}{3}\Delta_c$ and fine grid, $\Delta_f = \frac{1}{2}\Delta_c$ transfer functions are constructed to match that of the coarse grid.

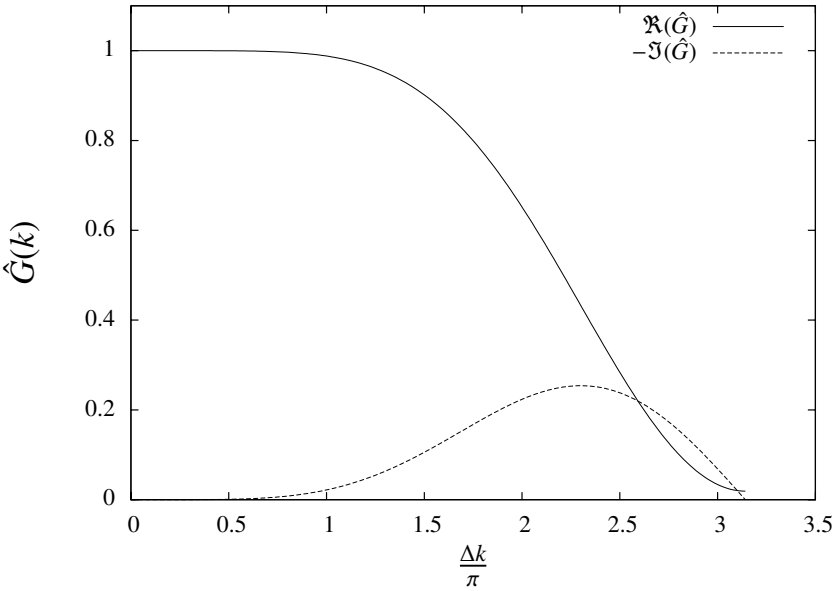

FIGURE 3. Real and imaginary parts of Fourier transform of asymmetric filtering operator on a six-point stencil, $K = 2$, $L = 3$ as defined in Eq.2.4.

$$L_{ij} = T_{ij} - \widehat{\tau_{ij}} = \widehat{\overline{u_i}\overline{u_j}} - \widehat{\bar{u}}_i\widehat{\bar{u}}_j \tag{2.8}$$

The standard Smagorinsky model $\tau^*_{ij}\ |\bar{S}_{ij}|\bar{S}_{ij}$ will also generate aliasing errors, and so in

Re_τ	N_x	N_y	N_z	Δx_f^+	Δz_f^+	Δy_f^+ (center)	L_x	L_z
180	64	64	64	71	24	20-25	4π	$\frac{4}{3}\pi$
180	96	96	96	71	24	20-25	4π	$\frac{4}{3}\pi$
180	128	128	128	71	24	20-25	4π	$\frac{4}{3}\pi$
395	64	64	64	78	39	50-60	2π	π
395	96	96	96	78	39	50-60	2π	π
395	128	128	128	78	39	50-60	2π	π

TABLE 1. Numerical parameters for channel flow simulations. N_x, N_y, N_z denote the number of grid points used in the streamwise, wall-normal, and spanwise directions respectively. L_x, L_z are the streamwise and spanwise domain length respectively, and a wall-normal size of 2 is used in all simulations. Δx_f^+ is the effective grid resolution in the streamwise direction in wall units based on filter width criteria of Vasilyev *et al.* (1998); Δz_f^+ and Δy_f^+ are the effective grid solutions in the streamwise direction and in the wall normal direction at the channel centerline, in wall units respectively. A range of Δy^+ resolutions near the centerline is given depending on the criteria used (Lund 1997).

order to avoid such a potential difficulty, the contribution of the subfilter stress model is also filtered. Therefore, the subfilter source term used is:

$$\tau_{ij} - \frac{1}{3}\tau_{kk}\delta_{ij} = -2\overline{(C\Delta^2)|\bar{S}_{ij}|\bar{S}_{ij}} \; . \tag{2.9}$$

3. Results and discussion

Channel flow simulations are performed at $Re_\tau = 180$ and $Re_\tau = 395$ using a fixed pressure gradient. At both Reynolds numbers, three LES are performed, listed in Table 1. The distribution of grid points in the wall normal direction is described by the hyperbolic tangent stretching function, Eq.2.7; the stretching parameter, γ, is fixed at 2.40 for all simulations.

The streamwise mean and the root mean square (rms) of the three velocity components are ensemble averaged. Figure 4 shows the mean streamwise velocity profiles at both Reynolds numbers. At both Reynolds numbers, the mean velocity profiles collapse between the two finer grid simulations, on the 96^3 and 128^3 meshes. The direct numerical simmulation (DNS) at $Re_\tau = 180$ is filtered to the same resolution that the corresponding LES. Even though the finer LES simulations collapse to a grid-independent prediction, the grid independent solution does not correspond to the filtered DNS results. As the grid is refined and the numerical error is decreased, the discrepancy between the grid independent LES and DNS is no longer attributed to the numerical error associated with the finite difference scheme. The discrepancy suggests that the potential incapability of

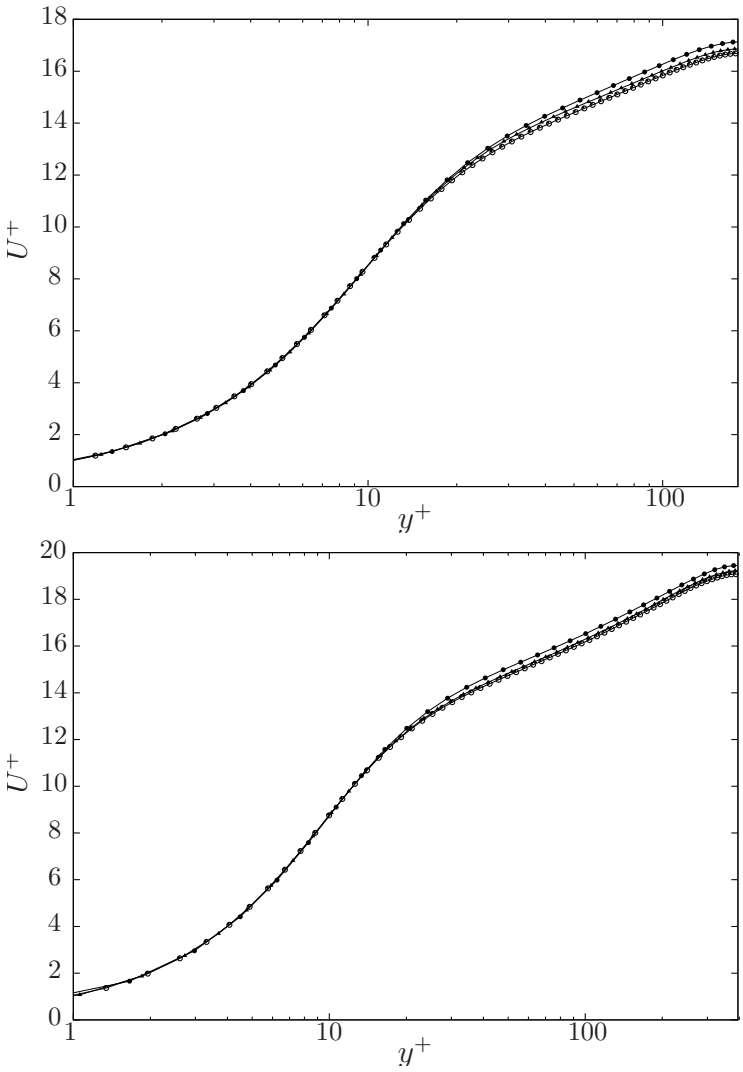

FIGURE 4. Mean streamwise velocity for a turbulent channel flow at $Re_\tau = 180$ (top) and $Re_\tau = 395$ (bottom) on 64^3 (•), 96^3 (▲), and 128^3 (∘) grids.

the subfilter closure model used.

Figures 5 and 6 show the rms velocity profiles for the streamwise, wall-normal, and spanwise directions, respectively. Near the channel centerline, the rms velocity profiles for the two finer LES calculations collapse well at both Reynolds numbers, similar to the behavior shown for the mean streamwise velocity. The collapse, however, is not as apparent in the near-wall peaks at both Reynolds numbers. The deviations in the predictions in the near-wall regions for the rms profiles is partially attributable to the statistical convergence. Although the high wavenumbers are damped by the explicit filtering, their amplitudes in time decay slowly. The deviations between the different grid levels have been observed to decrease as the solution is further integrated in time, but at a slow rate. The difficulty in matching the transfer functions of the asymmetric filters in the

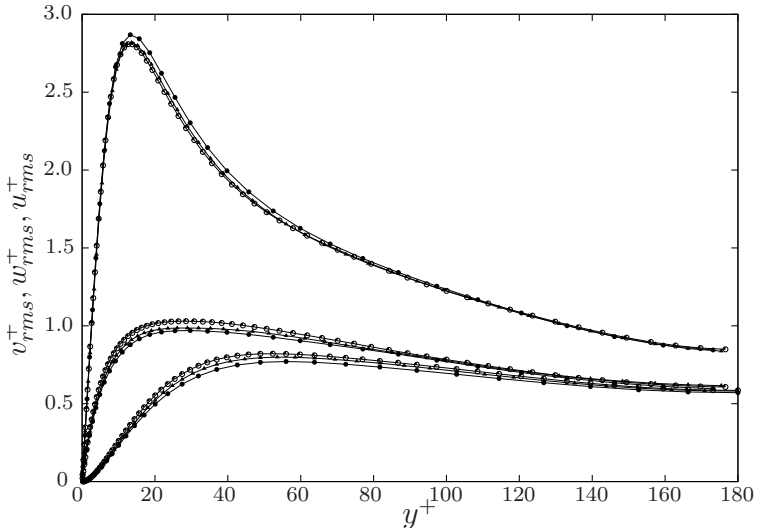

FIGURE 5. RMS velocity profiles for a turblent channel flow at $Re_\tau = 180$ using 64^3 (•), 96^3 (▲), and 128^3 (∘) grids.

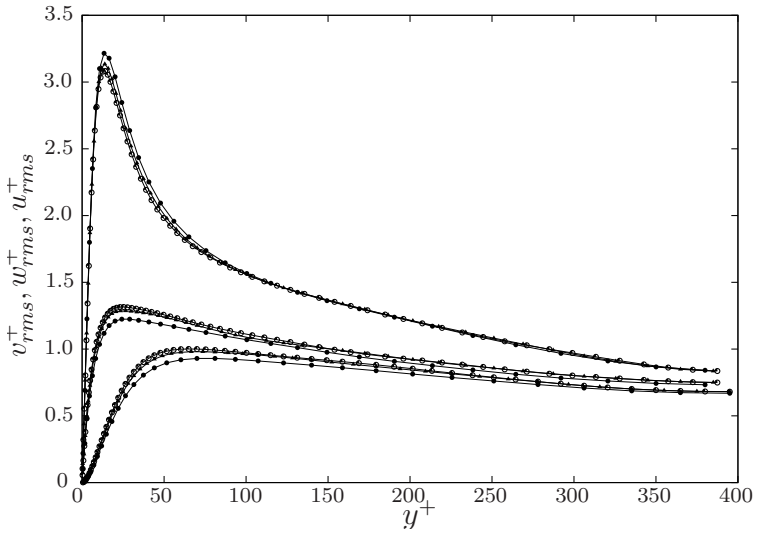

FIGURE 6. RMS velocity profiles for a turblent channel flow at $Re_\tau = 395$ using 64^3 (•), 96^3 (▲), and 128^3 (∘) grids.

near-wall region could also contribute to the observed deviations. In the finest LES simulations using 128^3 grid points, the first seven grid points away from the wall require asymmetric filtering.

A measure of the integrated relative error is proposed to estimate the difference between the wall-normal profiles:

$$E(f_1, f_2) = \frac{1}{2}\int_{-1}^{1} \frac{|f_1(y) - f_2(y)|}{|f_2(y)|} dy \; . \tag{3.1}$$

Re_τ	$E(\bar{u})$	$E(\bar{u}'_{rms})$	$E(\bar{v}'_{rms})$	$E(\bar{w}'_{rms})$
180	0.9%	0.8%	2.6%	2.1%
395	0.7%	0.7%	1.3%	0.9%

TABLE 2. Integrated relative difference, Eq.3.1, between simulations performed with 96^3 and 128^3 grid points for first and second order statistical quantities at $Re_\tau = 180$ and 395.

Table 2 shows the relative differences in the wall normal profiles between the simulations performed on the medium and fine meshes for both Reynolds numbers. Even though the same number of grid points is used in the simulations at both $Re_\tau = 180$ and $Re_\tau = 395$, the $Re_\tau = 395$ case shows a better collapse of the statistics to grid-independent levels. Because the Smagorinsky model is derived for high Reynolds number turbulence, it is possible that the subfilter closure model is better suited for the $Re_\tau = 395$ case as opposed to the $Re_\tau = 180$ simulations, and the poor convergence may be an indicator of a poor choice for a closure model for a given simulation. It is noted that this metric may be inappropriate for assessing the grid independence of different solutions. The commuting filter kernel derived by Vasilyev *et al.* is expressed as a linear combination of Dirac delta functions, and so it is not guaranteed that the LES solutions will converge pointwise to the true LES solution.

One-dimensional energy spectra in the streamwise and spanwise wavenumbers are also presented (Figures 7, 8). The nominal cutoff for all simulations, using the filter width criteria suggested by Lund (1997), is $k_{x,z} = 16$ in both the streamwise and spanwise directions. The 1-D energy spectra collapse for the LES simulations on 96^3 and 128^3 grids. The difference between the finer grids and the coarser simulation on 64^3 is due to the numerical error in the resolved scales. The collapsed spectra does not collapse well against the true DNS spectra, particularly for the E_{ww} quantities. The explicit filtered LES overpredicts the E_{ww} quantities even at the low wavenumbers that the simulations are supposed to resolve. However, the energy spectra confirm that the inclusion of an explicit filter does damp the higher frequencies and shows that the collapse of the first- and second- order statistics is not an artifact of the ensemble averaging.

Wall shear stress, $\frac{\partial u}{\partial y}$, contours are also presented in Figure 9 for the coarsest and finest explicit filtered LES calculations at $Re_\tau = 395$. In addition, Figure 10 depicts the same contours for an "implicit filtered" LES calculation using the same grid at the finest LES with 128^3 grid points. The structures associated with the skin friction are dominated by long streamwise streaks but smaller streamwise vortices also appear. The structures in the explicit filtered LES simulations are of the same size even as the grid is refined. The structures in the implicit filtered LES equation show the prescence of smaller scales and even small corrugations of the long streamwise streaks; this can be compared with the explicit filtered LES solution on the finest grid where these small scale corrguations are not present.

Although, the velocity profiles at both Reynolds numbers converge as the grid is refined, the output of the subfilter closure model does not. An ensemble average of the $\tau_{12} = \nu_t \bar{S}_{12}$ output of the Smagorinsky model is computed at $Re_\tau = 180$ and $Re_\tau = 395$ (Figure 11).

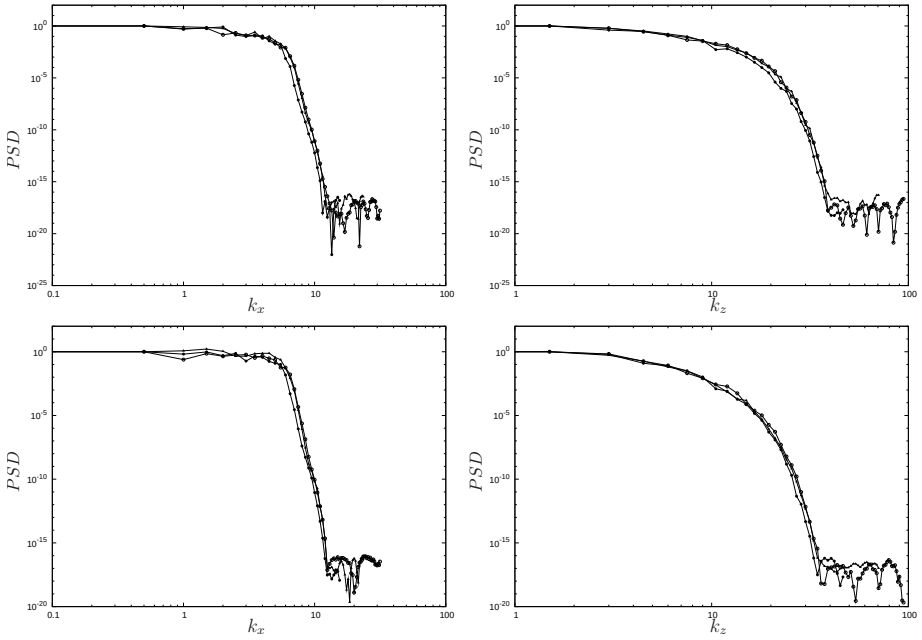

FIGURE 7. One dimensional energy spectra, $E_{uu}(k_x)$ (top left), $E_{uu}(k_z)$ (top right), $E_{ww}(k_x)$ (bottom left), and $E_{ww}(k_z)$ (bottom right) for $Re_\tau = 180$ channel flow on 64^3 (•), 96^3 (▲), and 128^3 (○) grids.

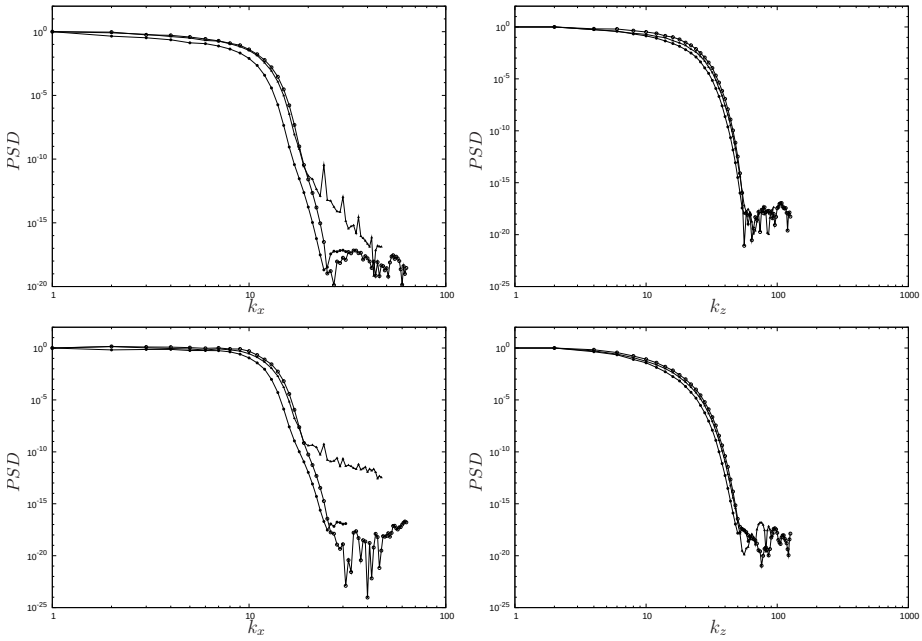

FIGURE 8. One dimensional energy spectra, $E_{uu}(k_x)$ (top left), $E_{uu}(k_z)$ (top right), $E_{ww}(k_x)$ (bottom left), and $E_{ww}(k_z)$ (bottom right) for $Re_\tau = 395$ channel flow on 64^3 (•), 96^3 (▲), and 128^3 (○) grids.

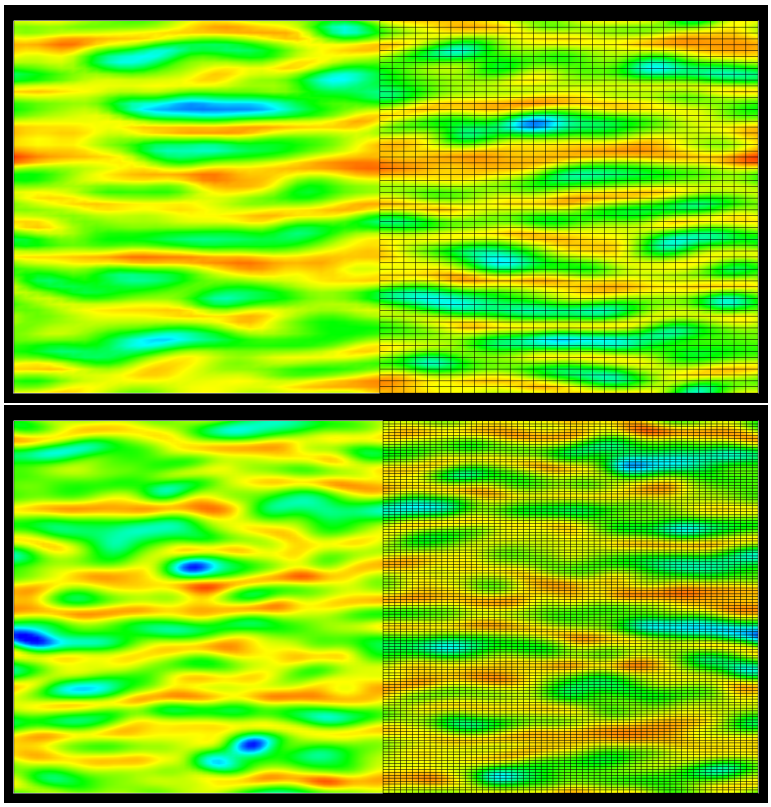

FIGURE 9. Wall shear stress, $\frac{\partial u}{\partial y}$, contours of an explicit filtered LES at $Re_\tau = 395$ for 64^3 (top) and 128^3 (bottom) grids.

The magnitude of the τ_{12} component between the coarsest and finest explicit filtered simulations differs by a factor of four roughly, though their profiles remain similar. It is possible that the output of the Smagorinksy model is amplified by the prescence of white noise at the higher wavenumbers; as the grid is refined and numerical errors are reduced, the output of the subfilter closure model also decreases. This would imply that models that are heavily biased to the higher wavenumbers may not be suitable for simulations with low-orders of accuracy.

4. Concluding remarks

Grid-independent statistics and spectra for a turbulent channel flow at different Reynolds numbers has been demonstrated in this study. The application of an explicit filter to the LES equations have enabled for an ambiguous separation of the scales that are resolved in the simulation, and consequently, those that must be modeled. Explicit filtering also offers hope of controlling the influence of numerical error in simulations, even if the order of the truncation error, $O(\Delta^q)$, is larger than the contribution of the smallest, dynamically relevant, physical scale, η. This result answers a few questions regarding the fidelity of LES, particularly the dependence of statistical estimates on the local grid size, raised by Pope (2004). While grid-independent solutions substantiate the consistency of LES as a numerical method, it does not answer questions regarding the dependence of

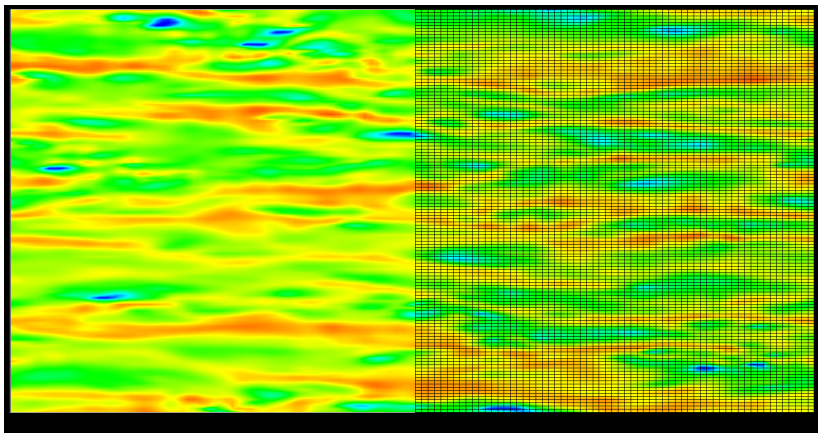

FIGURE 10. Wall shear stress, $\frac{\partial u}{\partial y}$, contours of an implicit filtered LES at $Re_\tau = 395$ for 128^3 grids.

statistical estimates on the filter width, Δ_f; a grid-independent solution obtained by an explicit filtered LES is not independent of the filter chosen or the filter width. In order to avoid supplanting ambiguity of LES predicitions due to the grid with dependence on the choice of filter, effective deconvolution approaches should be explored, either integrated into the simulation (Stolz *et al.* 2001) or in a post-processing context (Shu & Wong 1995).

Moreover, the failure of the grid-independent LES solutions to converge to a filtered DNS can now be directly attributable to errors in the subfilter stress closure model. In the "implicit filtered" LES framework, it was difficult to assess the fidelity of the closure model due to the observed sensitivity of the subgrid model to numerical errors. It is suggested that grid-independent solutions of the explicit filtered LES equations be used to determine the performance of a particular subfilter stress model when compared against a filtered DNS.

Although it is relatively easy to implement explicit filtering in LES simulations on structured grids, the prospect of explicit filtered LES on unstructured grids is more arduous. Although the commuting filters on unstructured meshes have been derived, they have yet to be implemented in any full 3-D LES simulation. While it is suggested that explicit filtering be utilized in unstructured grid simulations in order to increase their fidelity, it will be more difficult to find grid-independent solutions. Due to the particular implementation of the unstructured, commuting filters, it is more difficult to specify a filter width that can be preserved on different meshes. Further, the computational cost of implementing wide filters (greater than three times the local grid spacing) may become prohibitively expensive. However, explicit filtering on unstructred grids and in complex geometries remains an open question that deserves further attention.

REFERENCES

BIRINGEN, S. & REYNOLDS, W. 1981 Large-eddy simulation of the shear-free turbulent boundary layer. *J. Fluid Mech.* **103**, 53–63.

CHOW, F. & MOIN, P. 2003 A further study of numerical errors in large eddy simulation. *J. Comp. Phys* **184**, 366–380.

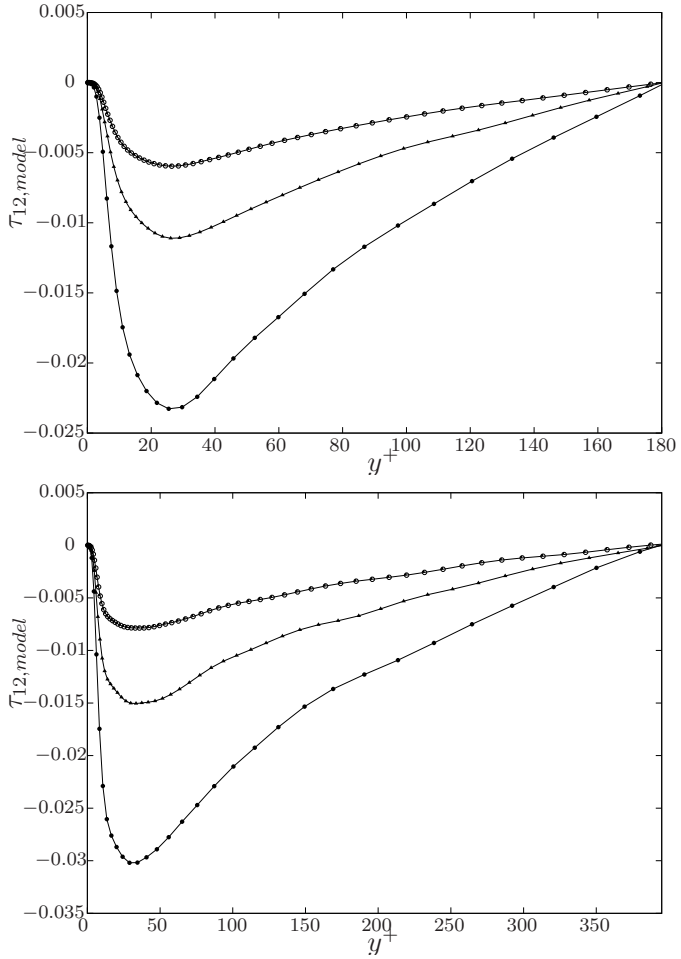

FIGURE 11. Ensembled averaged subfilter stress, $\tau_{12} = \nu_t \bar{S}_{12}$, at $Re_\tau = 180$ (left) and $Re_\tau = 395$ (right) using 64^3 (•), 96^3 (▲), and 128^3 (∘) grids.

DUKOWICZ, J. & DVINSKY, A. 1992 Approximate factorization as a high order splitting for incompressible flows. *J. Comp. Phys* **102**, 336–.

GERMANO, M., PIOMELLI, U., MOIN, P. & CABOT, W. 1991 A dynamic subgrid-scale eddy viscosity model. *Phys. of Fluids* **3** (7), 1760–1765.

GHOSAL, S. 1996 An analysis of numerical errors in large-eddy simulations of turbulence. *J. Comp. Phys* **125**, 187–206.

GULLBRAND, J. 2003 Grid-independent large-eddy simulation in turbulent channel flow using three-dimensional explicit filtering. *Center for Turbulence Research Ann. Res. Brief* pp. 331–342.

HASELBACHER, A. & VASILYEV, O. 2003 Commutattive discrete filtering on unstructured grids based on least-squares techniques. *J. Comp. Phys* **187**, 197–211.

KIM, J., MOIN, P. & MOSER, R. 1987 Turbulent statistics in a fully developed channel flow. *J. Fluid Mech.* **177**, 133–.

Kravchenko, A. & Moin, P. 1997 On the effect of numerical errors in large eddy simulation. *J. Comp. Phys* **131**, 310–322.

Kravchenko, A. & Moin, P. 2000 Numerical studies of flow over a circular cylinder at $re_d = 3900$. *Phys. of Fluids* **12**, 403–417.

Leonard, A. 1973 On the energy cascade in large-eddy simulations of turbulent flows. *Report TF-1, Thermosciences Division, Stanford University* .

Lund, T. 1997 On the use of discrete filters for large eddy simulation. *Center for Turbulence Research Ann. Res. Brief* pp. 83–95.

Lund, T. 2003 The use of explicit filters in large eddy simulation. *Comp. & Math.* **46**, 603–616.

Mahesh, K., Constantinescu, G., Apte, S., Ham, F. & Moin, P. 2006 Large-eddy simulation of reacting turbulent flows in complex geometries. *J. Appl. Mech.* **73** (3), 374–382.

Marsden, A., Vasilyev, O. & Moin, P. 2002 Construction of commutative filters for les on unstructured meshes. *J. Comp. Phys* **175**, 584–603.

Meyers, J. & Sagaut, P. 2007 Is plane-channel flow a friendly caes for the testing of large-eddy simulation subgrid-scale models? *Phys. of Fluids* **19**, 048105.

Moin, P. & Kim, J. 1982 Numerical investigation of turbulent channel flow. *J. Fluid Mech.* **118**, 341–377.

Morinishi, Y., Lund, T., Vasilyev, O. & Moin, P. 1998 Fully conservative higher order finite difference schemes for incompressible flow. *J. Comp. Phys* **143**, 90–124.

Moser, R., Kim, J. & Mansour, N. 1999 Direct numerical simulatino of turbulent channel flow. *Phys. of Fluids* **11** (4), 943–945.

Pope, S. 2004 Ten questions concernign the large-eddy simulation of turbulent flows. *New J. of Phys.* **6** (35), 1–24.

Rogallo, R. & Moin, P. 1984 Numerical simulation of turbulent flow. *Ann. Rev. of Fluid Mech.* **16**, 99–137.

Shu, C. & Wong, P. 1995 A note on the accuracy of spectral method applied to nonlinear conservation laws. *J. Sci. Comp.* **10** (3), 357–369.

Spezilae, C. 1985 Galilean invariance of subgrid-scale stress models in the large-eddy simulation of turbulence. *J. Fluid Mech.* **158**, 55–62.

Stolz, S., Adams, N. & Kleiser, L. 2001 An approximate deconvolution model for large-eddy simulation with application to incompressible wall-bounded flows. *Phys. of Fluids* **13** (4), 997–1015.

Vasilyev, O., Lund, T. & Moin, P. 1998 A general class of commutative filters for les in complex geometries. *J. Comp. Phys* **146**, 82–104.

Winckelmans, G., Wray, A., Vasilyev, O. & Jeanmart, H. 2001 Explicit-filtered large-eddy simulation using the tensor-diffusivity model supplemented by a dynamic smagorinsky term. *Phys. of Fluids* **13** (5), 1385–1403.

You, D., Wang, M., Moin, P. & Mittal, R. 2007 Large eddy simulation analysis of mechanisms for viscous losses in turbomachinery tip-clearance flow. *J. Fluid Mech.* **586**, 177–204.